Some interesting features of the Tb3+ magnetooptics in the paramagnetic garnets

ARTICLE *in* OPTICAL MATERIALS · MAY 2014

Impact Factor: 1.98 · DOI: 10.1016/j.optmat.2014.01.034

Optical Materials 36 (2014) 1101–1111

Contents lists available at ScienceDirect

Optical Materials

journal homepage: www.elsevier.com/locate/optmat

Some interesting features of the Tb^{3+} magnetooptics in the paramagnetic garnets

Uygun V. Valiev [a], John B. Gruber [b], Gary W. Burdick [c], Anvar K. Mukhammadiev [a], Dejun Fu [d,*], Vasiliy O. Pelenovich [d]

[a] Faculty of Physics, National University of Uzbekistan, Vuzgorodok, Tashkent 100174, Uzbekistan
[b] Department of Physics and Astronomy, The University of Texas at San Antonio, San Antonio, TX 78249, USA
[c] Department of Physics, Andrews University, Berrien Springs, MI 49104, USA
[d] School of Physics and Technology, Wuhan University, 430072 Wuhan, China

ARTICLE INFO

Article history:
Received 19 November 2013
Received in revised form 8 January 2014
Accepted 29 January 2014
Available online 4 March 2014

Keywords:
Luminescence
Magnetic circular polarization of luminescence
Magnetic circular dichroism
terbium–yttrium garnet gallate

ABSTRACT

The spectra of the absorption, luminescence, magnetic circular dichroism (MCD) and magnetic circular polarization of luminescence (MCPL) in the terbium–yttrium gallium garnet Tb^{3+}:$Y_3Ga_5O_{12}$ (Tb:YGG) have been studied within the visible and near ultraviolet (UV) spectral range for temperatures $T = 85$ and 300 K. The MCD spectrum observed within the UV absorption band for Tb:YGG is associated with spin- and parity-allowed electric-dipole $4f \rightarrow 5d$ transitions occurring between levels of the ground $^7F_6$ multiplet and the ^7D state of the excited $4f^{(7)}5d$ configuration of the Tb^{3+} ion. Analysis of the spectral and the temperature dependences of the magnetooptical and optical spectra has made it possible to identify magneto-optically-active $4f \rightarrow 4f$ transitions occurring between Stark sublevels of the $^5D_4$ and $^7F_5$ multiplets in Tb^{3+}:YGG. Quantum mechanical "mixing" of the three lowest energy Stark singlets in the excited $^5D_4$ multiplet by an external magnetic field H leads to the change of the circularly polarized luminescence line intensities. The Zeeman effect in the UV absorption band $^7F_6 \rightarrow {}^5L_{10}$ of Tb^{3+}:YGG at $T = 85$ K was also studied. The magnetic field dependence of the Zeeman splitting of some absorption lines is found to exhibit unusual behavior: as the magnetic field increases, the band splitting decreases rather than increases. A parameterized Hamiltonian defined to operate within the entire $4f^{(8)}$ ground electronic configuration of Tb^{3+} was used to model the experimental Stark levels, their irreducible representations (irreps.) and wave functions. The crystal-field parameters were determined using a Monte-Carlo method in which nine independent crystal-field parameters, were given random initial values and optimized using standard least-squares fitting between calculated and experimental levels. The final fitting standard deviation between 101 calculated and experimental Stark levels is 16.7 cm^{-1}.

1. Introduction

The series of paramagnetic trivalent rare-earth (RE^{3+}) ions [1], characterized by an unfilled shell of 4*f*-electrons, are relatively easy to investigate optically as dopants in insulating garnet systems, such as the yttrium aluminum or yttrium gallium garnets ($Y_3Al_5O_{12}$ or $Y_3Ga_5O_{12}$). These compounds, also known as aluminates and gallates, respectively, have demonstrated useful electronic applications when doped with Tb^{3+}, including highly effective infrared stimulated emission [2] that involves the crystal-field (CF) split electronic transitions between the $^7F_5$ and $^5F_6$ states of Tb^{3+} ($4f^{(8)}$). Of the members of the rare-earth series, Tb^{3+} in particular exhibits unique optical and magnetic properties that are of interest for the creation of intriguing and complex photonic systems. As insulating materials, the Tb^{3+} garnets serve well as optical modulators and filters for the visible region due to their high magneto-optical Faraday rotation and low optical absorption because of the forbidden nature of allowed electric-dipole transitions within the $4f^{(n)}$ subshell [3].

Several of us have reported previously both the spectroscopy and potential photonic applications for Tb^{3+} doped garnets [4]. That work also included detailed analysis of the CF splitting of the $^{2S+1}L_J$ manifolds of the Tb^{3+} energy manifolds. Trivalent terbium replaces Y^{3+} in sites of D_2 symmetry in the garnet structure. As Tb^{3+} has an even number of equivalent 4*f* electrons, the CF of D_2 symmetry is composed of $(2J + 1)$ non-degenerate energy (Stark) levels for each isolated manifold of Tb^{3+} [4,5]. However, especially within

* Corresponding author. Tel.: +86 2768753587.
E-mail address: 592563827@qq.com (D. Fu).

http://dx.doi.org/10.1016/j.optmat.2014.01.034
0925-3467/

the manifolds with large J, some of these Stark levels are nearly degenerate. In the presence of an external magnetic field H, the wavefunctions of two such nearly degenerate Stark levels are "mixed," and these levels can form what is called a "quasi-doublet" state [6]. The magnetic [6] and magneto-optical [7] character of these "quasi-degenerate" states as revealed by magnetic and polarization-optical studies has been the source of interesting and novel applications. As a consequence of having an even number of electrons in the unfilled $4f^{(n)}$-electronic shell, the Tb^{3+} ion has become a successful ionic probe useful for studies of magneto-optical spectroscopy and in the magnetism of rare-earth ions in solid state hosts.

Results of previous magneto-optical studies of the paramagnetic terbium-containing garnets, primarily of the terbium–yttrium aluminum Tb:YAG garnet, performed in the near ultraviolet (UV) and visible spectral regions [7–9], can be formulated as follows.

(1) A prevailing contribution of the allowed $4f \rightarrow 5d$ transitions to the magneto-optics of Tb^{3+} ions in the YAG garnet is observed in the near UV and visible spectra.
(2) Magneto-optical effects observed for the non-Kramers Tb^{3+} ions in the YAG garnet and associated with the parity-forbidden $4f \rightarrow 4f$ transitions are described taking into account the selection rules for the "forced" electric-dipole transitions [1,2,5,7].
(3) A dominant contribution to the mechanism of removal of the parity prohibition from the $4f \rightarrow 4f$ transitions in Tb:YAG garnet is made by "mixing" of an odd symmetrical component of the CF of D_2 symmetry of the excited configuration $4f^{(7)}5d$ with the states of the ground $4f^{(8)}$ configuration of the Tb^{3+} ion.
(4) Large magneto-optical effects observed in Tb:YAG in the spectral range of standard UV radiation sources (several UV lasers and Xe lamp) can be used to develop powerful magneto-optical modulators and optical isolators.

Similar studies of optical and magneto-optical properties (particularly in the UV range) of terbium–yttrium gallium garnets Tb^{3+}:$Y_3Ga_5O_{12}$ (Tb:YGG) have not previously been done though the nature of the garnet host can substantially affect the MOA of the electron transitions in Tb^{3+} ions.

In the present study, we investigate systematically the different mechanisms of the MOA of the Tb^{3+} ions in the gallate system in order to better understand the nature of the significant magneto-optical effects observed in the different garnet hosts (gallates and aluminates). The interpretation of the experimental data is supported by CF calculations for all the mutiplet manifolds of Tb^{3+} in YGG up to 29,150 cm^{-1}. The CF calculations use a parameterized Hamiltonian:

$$\widehat{H}_{CF} = \sum_{k,q} B_q^k C_q^{(k)}$$

for the $4f^{(8)}$ electron shell of the Tb^{3+} ion located in one of the non-equivalent positions (c-sites) in the YGG lattice. In D_2 symmetry, nine real CF parameters B_q^k are allowed (Table 1). Calculations of the Tb^{3+} spectrum include J–J "mixing" of the wave functions in the $|J,M_J>$ basis (Table 2). In D_2 symmetry, there are six possible coordinate system orientations, with the quantization z-axis oriented along any of the three inequivalent c_2 symmetry axes of the crystal, and the x-axis oriented along either of the two remaining c_2 symmetry axes. This results in six different (but spectroscopically indistinguishable) crystal field parametrizations. Table 1 presents all six of these crystal field parametrizations in "modified" Morrison–Leavitt notation [10], along with the fitted "atomic" parameters necessary to calculate energy levels for the ground $4f^{(8)}$-electronic configuration of Tb^{3+}. Values for the atomic and crystal-field parameters were determined using a Monte-Carlo method in which the nine independent B_q^k crystal-field parameters were given random initial values and optimized using standard least-squares fitting between calculated and experimental levels. Statistical uncertainties are given in parentheses after each parameter value; atomic parameters given in brackets were held fixed at previously determined values. The final fitting standard deviation between 101 calculated to experimental Stark levels is 16.7 cm^{-1} (rms error = 14.9 cm^{-1}).

The directions and notations of axes in a local coordinate system (c – sites) correspond to one of the crystallography-nonequivalent positions of the Tb^{3+} ion in the YGG structure, chosen in such a way that the parameterization z – axis is parallel to the [0 0 1] cubic crystal axis and perpendicular to the xy – plane of the local coordinate system. This orientation is represented by the crystal field parameters given as "Set 1" (top sign) in Table 1. To evaluate the results of the magneto-optical measurements, we used the wave functions which were transformed into the coordinates used by Guillot et al. [11] for Tb^{3+}in $Y_3Ga_5O_{12}$ and Bayerer et al. [5] for Tb^{3+} in $Y_3Al_5O_{12}$, for which x' – axis was chosen parallel to the [0 0 1] cubic crystal axis, perpendicular to the $y'z'$ – plane. The coordinate transformation of the wave functions was carried out using the Wigner D – functions [7,12]. If we use prime labels Γ_n' to identify the symmetry labels, i.e. irreducible representations (irreps.), used by Guillot et al. [11] and Bayerer et al. [5], our labels will relate as $\Gamma_1 = \Gamma_1'$, $\Gamma_2 = \Gamma_3'$, $\Gamma_3 = \Gamma_4'$ and $\Gamma_4 = \Gamma_2'$. This orientation is represented by the crystal field parameters given as "Set 3" (top sign) in Table 1. The wave functions and their irreps in our coordinate system are given in columns 3 and 4 of Table 2. The transformed wave functions are listed in columns 5 and 6, with the experimental energy of the Stark levels given in column 8 of the table. The set of wave functions listed in columns 5 and 6 were used in the following analysis of the magneto-optical data.

2. Measurement technique and samples

Single crystal Tb:YAG ($Tb_{0.2}Y_{2.8}Al_5O_{12}$) was grown using a high-temperature Czochralski method. The growth direction of the Tb:YAG sample was along the [0 0 1] – axis of the cubic garnet crystal. We also investigated the spectra of single-crystal YGG ($Y_3Ga_5O_{12}$) doped with a small concentration of Tb^{3+} ions (~1.0 weight%) oriented along an arbitrary crystallographic direction and TbGG ($Tb_3Ga_5O_{12}$) single-crystal oriented along (1 1 0) crystallographic direction. A fourth sample studied was a thin epitaxial film of terbium–yttrium gallate $Tb_{0.6}Y_{2.4}Ga_5O_{12}$ grown on a gadolinium gallate GGG ($Gd_3Ga_5O_{12}$) substrate oriented along the crystallographic direction [1 1 1]. The crystal structure of all four samples investigated was confirmed by XRD methods [13].

Both the optical and magneto-optical spectra reported in the present study were taken at 85 K and 300 K using a liquid nitrogen Dewar. To resolve the structure observed in the photoluminescence (fluorescence) as well as in the absorption spectra, we used a high-resolution diffraction monochromator (MDR model 23, "LOMO", St. Petersburg, Russia). Detection of the absorption ultraviolet (UV) spectra was made using photomultiplier tubes sensitized by a technique described earlier that stabilizes the average photomultiplier current at a constant level while scanning over a given line shape [14]. The wavelength range covered in both emission and absorption experiments was approximately from 240 nm to 545 nm (41,650 cm^{-1} to 18,350 cm^{-1}, respectively) with an average instrumental spectral resolution of 0.03 nm (~3.8 cm^{-1}) for the absorption spectra and 0.05 nm (~1.7 cm^{-1}) for the fluorescence measurements.

Table 1
Atomic and Crystal-field energy parameters (in cm^{-1}) for Tb^{3+} in YGG. Six alternative crystal-field parameter sets are presented using modified Morrison and Leavitt notation. "Set 1" (top sign) corresponds to the orientation having z || axis [001] of crystal; "Set 3" (top sign) corresponds to the orientation having x' || axis [001] of crystal.

Atomic parameter	Value (cm^{-1})	Crystal field parameter	Value (cm^{-1}) Set 1	Value (cm^{-1}) Set 2	Value (cm^{-1}) Set 3
E_{avg}	68,371 (54)	B_0^2	108 (32)	−148 (33)	40 (20)
F^2	88,696 (126)	B_2^2	∓77 (18)	∓28 (17)	±104 (25)
F^4	63,647 (264)	B_0^4	−243 (45)	224 (48)	−2367 (30)
F^6	46,370 (128)	B_2^4	∓1639 (26)	±1344 (28)	±295 (38)
α	[18.40]	B_4^4	−937 (33)	−1328 (28)	840 (29)
β	−660 (26)	B_0^6	−1314 (56)	−712 (53)	696 (45)
γ	[1650]	B_2^6	∓396 (38)	±438 (38)	∓199 (41)
T^2	[320]	B_4^6	597 (34)	758 (37)	1134 (34)
T^3	[40]	B_6^6	∓474 (36)	±763 (36)	∓183 (41)
T^4	[50]				
T^6	[−395]				
T^7	[303]				
T^8	[317]				
ζ	1678 (4)				
M^0	[2.39]				
M^2	[$0.56M^0$]				
M^4	[$0.31M^0$]				
P^2	381 (44)				
P^4	[$0.50P^2$]				
P^6	[$0.10P^2$]				

In both types of magneto-optical experiments, magnetic circular dichroism (MCD) and magnetic circular polarization of luminescence (MCPL), a high-aperture geometry was used, in which so called "natural" (i.e. completely unpolarized) light radiation was projected onto the sample positioned in a longitudinal (relative to the lig $I_{\pm}\frac{I_+-I_-}{I_++I_-}$ ht propagation) external magnetic field H. Ultraviolet light between 240 nm and 400 nm (41,650 cm^{-1} to 25,000 cm^{-1}, respectively) was used to excite the "blue" and "green" luminescence of Tb:YAG and Tb:YGG, respectively. The MCPL spectra were measured in the vicinity of the radiative transitions: $^5D_4 \rightarrow {}^7F_6$ and $^5D_4 \rightarrow {}^7F_5$. A Xe-lamp (200 W) was used to measure the MCD spectra in the vicinity of the UV absorption band observed in a thin epitaxial film of terbium–yttrium gallate $Tb_{0.6}Y_{2.4}Ga_5O_{12}$. The circularity degree, P, of the partially polarized emitted (MCPL) or transmitted (MCD) light is given by the ratio [15,16]: $P = \frac{I_+-I_-}{I_++I_-}$ where $I_{\pm}$ are the intensities of the clockwise- and counter-clockwise polarized components of light. P values were measured with a high-sensitive technique of light polarization modulation [16] that involved a photoelastic modulator with optical feedback designed by some of the present authors [17].

The Zeeman effect (in a longitudinal geometry) was studied in the luminescence spectra of the paramagnetic garnets Tb:YGG and Tb:YAG ($Tb_{0.2}Y_{2.8}Al_5O_{12}$) at $T = 85$ K in a magnetic field $H = 0.7\ T$ (7 kOe) applied along an arbitrary crystallographic

Table 2
Numerically calculated energy levels (cm^{-1}) of the $^7F_6$, $^7F_5$, $^5D_4$ and $^5L_{10}$ multiplets of Tb^{3+} in YGG, along with irreps. (Γ_n) identifiers and largest wavefunction components (>10%) for each energy level.

$^{2S+1}L_J$	Level #	Wavefunctions in the $\|J, M_J\rangle$ basis				Energy (cm^{-1}) calc.	Energy (cm^{-1}) exp. [18]
		Local axis – z || axis [001] of crystal		Local axis – x' || axis [001] of crystal			
		Γ_n	Wavefunctions	Γ'_n	Wavefunctions		
$^7F_6$	1	Γ_1	$\Psi_1 = 0.686\ \|6, 0\rangle - 0.478(\|6, 2\rangle + \|6, -2\rangle)$	Γ'_1	$\Psi_1 = -0.688(\|6, 6\rangle + \|6, -6\rangle)$	9.4	0
	2	Γ_2	$\Psi_2 = -0.631(\|6, 1\rangle - \|6, -1\rangle)$	Γ'_3	$\Psi_2 = 0.689(\|6, 6\rangle - \|6, -6\rangle)$	9.6	0
$^7F_5$	14	Γ_2	$\Psi_{14} = -0.614(\|5, 3\rangle + \|5, -3\rangle)$	Γ'_3	$\Psi_{14} = 0.647(\|5, 4\rangle + \|5, -4\rangle)$	2043	2052
	15	Γ_1	$\Psi_{15} = 0.618(\|5, 2\rangle - \|5, -2\rangle) - 0.320(\|5, 4\rangle - \|5, -4\rangle)$	Γ'_1	$\Psi_{15} = 0.695(\|5, 4\rangle - \|5, -4\rangle)$	2057	2075
	16	Γ_4	$\Psi_{16} = 0.484(\|5, 5\rangle - \|5, -5\rangle) - 0.450(\|5, 3\rangle - \|5, -3\rangle)$	Γ'_2	$\Psi_{16} = -0.652(\|5, 3\rangle + \|5, -3\rangle)$	2083	2108
	17	Γ_3	$\Psi_{17} = -0.523(\|5, 2\rangle + \|5, -2\rangle) - 0.500\ \|5, 0\rangle$	Γ'_4	$\Psi_{17} = 0.576(\|5, 3\rangle - \|5, -3\rangle) - 0.351(\|5, 1\rangle - \|5, -1\rangle)$	2100	2113
$^5D(3)_4$	50	Γ_3	$\Psi_{50} = 0.420(\|(3)4, 2\rangle - \|(3)4, -2\rangle) - 0.333(\|(1)4, 2\rangle - \|(1)4, -2\rangle)$	Γ'_4	$\Psi_{50} = 0.499(\|(3)4, 3\rangle + \|(3)4, -3\rangle) + 0.396(\|(1)4, 3\rangle + \|(1)4, -3\rangle)$	20471.7	20,475
	51	Γ_4	$\Psi_{51} = -0.391(\|(3)4, 1\rangle + \|(3)4, -1\rangle) + 0.338(\|(3)4, 3\rangle + \|(3)4, -3\rangle) + 0.310(\|(1)4, 1\rangle + \|(1)4, -1\rangle)$	Γ'_2	$\Psi_{51} = -0.512(\|(3)4, 3\rangle - \|(3)4, -3\rangle) + 0.406(\|(1)4, 3\rangle - \|(1)4, -3\rangle)$	20472.0	20,475
	52	Γ_1	$\Psi_{52} = -0.351(\|(3)4, 4\rangle + \|(3)4, -4\rangle) + 0.345\ \|(3)4, 0\rangle$	Γ'_1	$\Psi_{52} = -0.514(\|(3)4, 2\rangle + \|(3)4, -2\rangle) + 0.408(\|(1)4, 2\rangle + \|(1)4, -2\rangle)$	20,485	20,493
$^5L_{10}$	79	Γ_3	$\Psi_{79} = 0.428(\|10, 6\rangle - \|10, -6\rangle) - 0.362(\|10, 8\rangle - \|10, -8\rangle)$	Γ'_4	$\Psi_{79} = -0.574(\|10, 7\rangle + \|10, -7\rangle)$	26,721	26,718
	80	Γ_1	$\Psi_{80} = 0.441(\|10, 8\rangle + \|10, -8\rangle) - 0.403(\|10, 6\rangle + \|10, -6\rangle)$	Γ'_1	$\Psi_{80} = -0.573(\|10, 6\rangle + \|10, -6\rangle) - 0.327(\|10, 8\rangle + \|10, -8\rangle)$	26,728	26,738
	81	Γ_4	$\Psi_{81} = -0.407(\|10, 7\rangle + \|10, -7\rangle)$	Γ'_2	$\Psi_{81} = 0.582(\|10, 7\rangle - \|10, -7\rangle)$	26,737	26,747
	82	Γ_2	$\Psi_{82} = -0.502(\|10, 7\rangle - \|10, -7\rangle) + 0.309(\|10, 9\rangle - \|10, -9\rangle)$	Γ'_3	$\Psi_{82} = 0.595(\|10, 6\rangle - \|10, -6\rangle)$	26,738	26,755

direction or the [001] crystallographic directions, respectively. In our experiments we also examined opposite circularly polarized components of absorption lines in a longitudinal magnetic field; these components were separated with a phase-shifting "$\lambda/4$" mica plate and a linear polarizer for the measuring of the Zeeman effect. A fused silica Fresnel rhomb with an angle of about 52° served as the "$\lambda/4$" plate for the observing of the UV absorption longitudinal Zeeman spectra in TbGG in a magnetic field $H = 0.7$ T applied along (1 1 0) crystallographic direction [18]. The relative error in measuring the absorption and luminescence spectra in all experiments did not exceed about 2–3%.

3. Results and discussion

3.1. UV spectra of MCD and absorption of the Tb^{3+} ions in YGG

The experimental optical absorption spectrum of $Tb_{0.6}Y_{2.4}Ga_5O_{12}$ thin film in the spectral range between 32,000 E_1 cm^{-1} and 41,650 cm^{-1} taken at $T = 85$ K is presented in Fig. 1, which shows a broad structureless asymmetrical band of strong absorption centered about 38,000 cm^{-1}. In order to explain the observed asymmetry of this band, we have decomposed the band into three elementary Gaussian components, which are presented by the dotted lines in Fig. 1. This decomposition shows that this band can be mainly formed by the superposition of two Gaussian contours at = 35,190 cm^{-1} and = 38,000 cm^{-1}.

The large (3000 cm^{-1}) value of the FWHM (Full Width at Half Maximum) observed for the UV absorption line $E_2 = 38{,}000$ cm^{-1}, along with the large value of the absorption coefficient (~1000 cm^{-1}) measured at the maximum of this line, together with the fact that MCD is observed only for (Fig. 1) indicate that this line is associated with spin- and parity-allowed electric-dipole (ED) interconfigurational $4f \rightarrow 5d$ transitions. These transitions occur between the ground $^7F_6$ multiplet and the "optically" allowed state ^7D formed due to the electrostatic interaction between the $5d$-electron and the lowest state ^8S of the $4f^{(7)}$ configuration of the Tb^{3+} ion "core" in YGG structure. By contrast, the absorption band observed at = 35,190 cm^{-1}, which has no MCD signal, apparently can be associated with $^1S_0 \rightarrow {}^3P_1$ electronic transitions in the impurity Pb^{2+} ions [19].

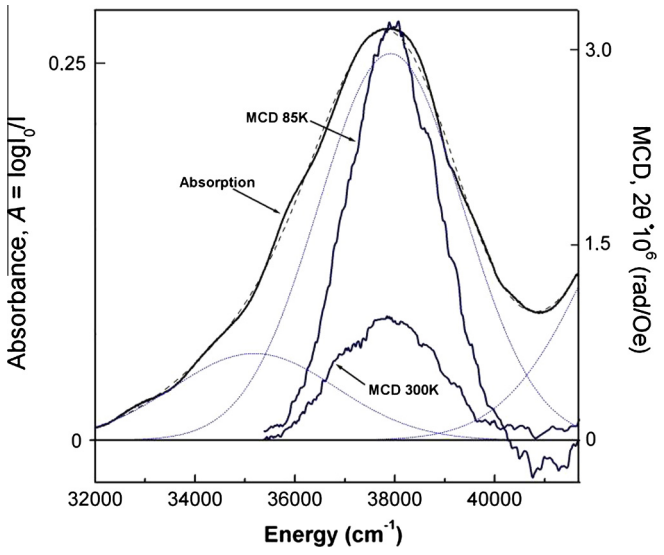

Fig. 1. MCD spectra of $Tb_{0.6}Y_{2.4}Ga_5O_{12}$ epitaxial thin film recorded at $T = 85$ K (solid line) and 300 K (solid line) within the absorption band (solid line) near 38000 cm^{-1} in an external field $H = 0.5$ T oriented along the crystallographic direction [1 1 1]. Decomposition of the optical absorption band at 38,000 cm^{-1} observed at $T = 85$ K is obtained using three Gaussian line profiles (dotted lines). Dashed lines represent the reconstructed optical absorption dependence. The optical absorption and MCD data were measured using the same epitaxial garnet film.

The measured spectral dependences of MCD in $Tb_{0.6}Y_{2.4}Ga_5O_{12}$ are presented in Fig. 1 for the intense optical absorption band between 35,500 cm^{-1} and 41,650 cm^{-1} in an external magnetic field $H = 0.5$ T at $T = 85$ K and 300 K. It is easy to see that the observed contour of the MCD spectrum line proves to be practically the same as that of the contour of intense optical absorption line = 38,000 cm^{-1} (Fig. 1). When the temperature drops from 300 K down to 85 K, its area (more exactly, the zero-order moment of MCD band, $<\theta>_0 = \int_0^\infty \frac{\theta}{\omega} d\omega$ [19,20]) increases, i.e. the zero moment of the MCD band associated with an absorption transition $4f^{(8)} \rightarrow 4f^{(7)}5d$ varies inversely with temperature (~$1/T$) in the 85–300 K temperature range, indicating the dominant contribution of the "paramagnetic" C-term to the UV magneto-optical activity (MOA).

It is well-known that the "paramagnetic" contribution of the MOA is proportional to the difference in the Boltzmann populations of the RE-ion ground state CF splitting components in an external magnetic field H and, therefore, is a function of inverse temperature (~$1/T$) [3,7,20,21]. In MCD spectroscopy, obtaining detailed information regarding the values of the "paramagnetic" C-term usually involves numerical integration of the MCD spectral dependence within the absorption band of the magneto-active ion – the so called method of MCD moments [20,21]. On the other hand, the C/D ratio unambiguously defines the "paramagnetic" MOA and can identify the ground state magnetic moment of the ion under consideration [20]. D is the "dipole strength" of the optical transition (proportional to the oscillator strength f) between ground and exited states of magneto-active ion [20,21].

Let's consider the simple model (in the free ion approximation) of the ED transition from the states of the Tb^{3+} ion ground $^7F_6$ multiplet to the lowest states of its $4f^{(7)}5d$ configuration (the $^7D_5$ multiplet) allowed by the selection rules for the calculation of C/D ratio value. It is well-known that the MCD spectrum in the energy range of an isolated electronic absorption band can be described by the following expression for the Faraday ellipticity, θ_F (per unit length), which is conditioned by the MCD and is obtained in the approximation $kT \ll \mu_B H$ [20]:

$$\theta_F = \frac{1}{4}(\alpha_+ - \alpha_-) = \gamma \mu_B H \left[\frac{A}{\hbar} \cdot \frac{df}{dv} + \left(\frac{C}{kT} + B\right) f\right] \quad (1)$$

where $f = f(v, v_0)$ is the function of the absorption band contour; v is the wave number (in cm^{-1}); γ is a constant [20]; k is the Boltzmann constant (= 0.695 cm^{-1}/K); μ_B is the Bohr magneton (= 4.67 10^{-5} cm^{-1}/Oe); and α_+ and α_- are the absorption coefficients for clockwise- and counterclockwise circular polarization radiation.

The expressions for C in Eq. (1) and for the optical transition dipole strength, D, can be determined as [20,21]:

$$C = \frac{1}{d_0} \sum_{a,b} \left[|< a|\hat{d}_-|b>|^2 - |< a|\hat{d}_+|b>|^2 \right] < a|\hat{\mu}_Z|a> \quad (2)$$

$$D = \frac{1}{2d_0} \sum_{a,b} \left[|< a|\hat{d}_-|b>|^2 + |< a|\hat{d}_+|b>|^2 \right] \quad (3)$$

where $\hat{d}_\pm = e(\hat{x} \pm i\hat{y})$ are the operators of the dipole moment cyclic coordinates, $\hat{\mu} = -g_0 \mu_B \hat{J}_Z$ is the operator of the z-projection of the magnetic moment, μ_B is the Bohr magneton, d_0 is the degeneracy order of the ground state, and $|a> = |L_0 S_0 J_0 M_{J_0}>$ and $|b> = |LS_0 J M_J>$ are the wave functions of the ground $|a>$ and excited $|b>$ states of the optical transition, respectively.

The first term involving A in Eq. (1) defines a temperature-independent "diamagnetic" contribution to the MCD due to the Zeeman splitting of the sublevels of the final electronic state

combining in the optical transition. The second term describes a contribution of the paramagnetic C-term of the MCD dependent on the splitting of occupied sublevels of the initial electronic state in the external magnetic field H. The third term involving B in Eq. (1) describes a contribution arising from "mixing" of the electronic states by an external magnetic field H [3,20,21].

Taking into account the selection rule in the Eqs. (2) and (3), and carrying out the appropriate summation over all possible transitions between the a and b states, we obtain $C/D = g_0(J_0 + 1)\text{-}\mu_B = 10.5\mu_B$, where $g_0 = 1.5$ and $J_0 = 6$ are the g-factor and the total angular moment of the $^7F_6$ multiplet in the Tb^{3+} ion, respectively.

From an experimental point of view, it is convenient to use the dimensionless terms of the optical absorbance A and the magneto-optical absorbance ΔA, which are defined by the expressions [21]:

$$A = \log\frac{I_0}{I(l)} \text{ and } \theta_F = 1.1512 \cdot \Delta A \tag{4}$$

In Eq. (4), θ_F is the Faraday ellipticity (in radians) due to the MCD:

$$P = \frac{I_+ - I_-}{I_+ + I_-} = \sin 2\theta_F. \tag{5}$$

where P is the circularity degree of the elliptically-polarized light passing through the magnetized sample of thickness l.

Then, owing to the linear increase of the zero-order moment of the MCD band $\langle\theta\rangle_0$ ($\sim 1/T$) with the temperature decrease from 300 to 85 K, the magnitudes of both the C/D and B/D ratios (in units of μ_B) can be determined by the integration of the MCD and absorption bands at the different temperatures as [21]:

$$\frac{1}{D}\left(\frac{C}{kT} + B\right) = 2.14\frac{\langle \Delta A/H\rangle_0}{\langle A\rangle_0} \tag{6}$$

where the zero-order moments for absorbance and MCD are defined relative to the MCD or absorption band centers of "gravity", which is about 38,000 cm^{-1} (see also [20]).

Analysis of the experimental data given in Fig. 1 with Eq. (6) shows that the C/D ratio value is equal to 8.9 μ_B for the Tb^{3+} ion in YGG structure. At the same time, the value of the "mixing" contribution to the MOA (B-term [3,20,21]) of Tb^{3+} in this structure is negligible. Note that the experimentally found C/D ratio is in a reasonable agreement with the C/D theoretical estimate of 10.5μ_B, made using a free RE-ion approximation for the magneto-optically-active ED transition $4f^{(8)}(^7F_6) \rightarrow 4f^{(7)}5d(^7D_5)$, confirming identification of the $E_2 = 38{,}000$ cm^{-1} transition. For comparison, the value of the Tb^{3+} magnetic moment in yttrium–gallium garnet, found from magnetic measurements, is equal to 9.78 [22]. This confirms the relation between the "paramagnetic" MOA and the magnetic properties of the RE-ion.

3.2. MCPL and Zeeman spectra of Tb^{3+} containing paramagnetic garnets

The spectral dependences of the MCPL degree, $P = \frac{I_+ - I_-}{I_+ + I_-}$, and the longitudinal Zeeman effect of Tb^{3+} containing paramagnetic garnets (YAG and YGG) were recorded for the luminescence bands associated with $4f \rightarrow 4f$ transitions $^5D_4 \rightarrow {}^7F_6$ ($Tb_{0.2}Y_{2.8}Al_5O_{12}$) and $^5D_4 \rightarrow {}^7F_5$ (Tb:YGG) at $T = 85$ K. Fig. 2 compares the MCPL degree and fluorescence spectra for the $^5D_4 \rightarrow {}^7F_6$ transition in Tb:YAG, while Fig. 3 compares the MCPL degree and fluorescence spectra for the $^5D_4 \rightarrow {}^7F_5$ transition of Tb:YGG. A comparison of the energies of emission lines 1, 2, …, 7 observed experimentally at $T = 85$ K (Fig. 3) with the theoretical energy level diagram of the Tb^{3+}ion in D_2 symmetry allows symmetry identification of the corresponding emissive transitions for $^5D_4 \rightarrow {}^7F_5$ (see Fig. 4). Symmetry labels (irreps.) of the Stark levels reported in the present

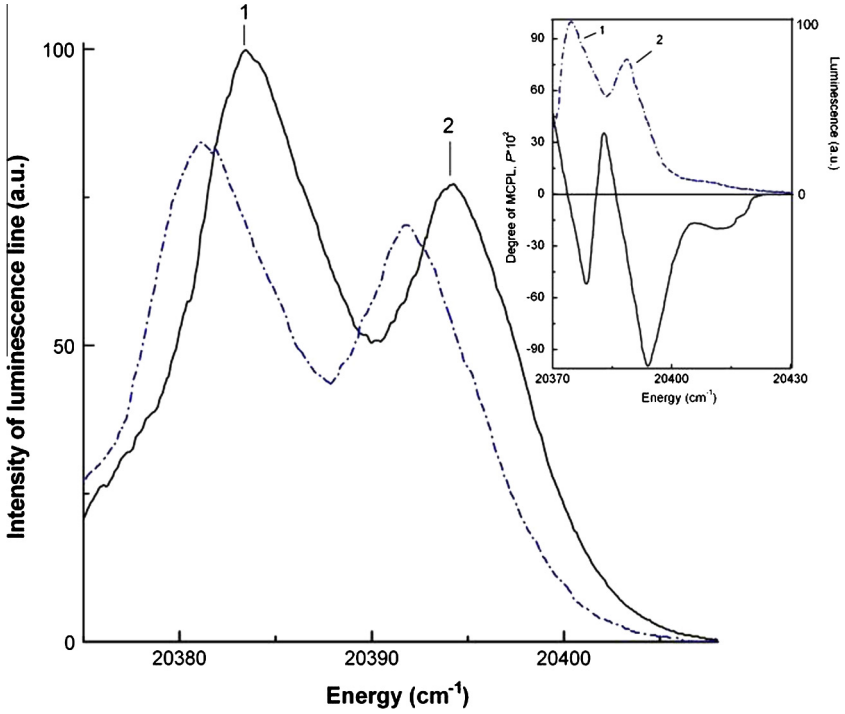

Fig. 2. Comparison of the MCPL degree P spectrum (solid line) with the luminescence (fluorescence) spectrum (dashed line) measured within the emissive $^5D_4 \rightarrow {}^7F_6$ band in the $Tb_{0.2}Y_{2.8}Al_5O_{12}$ (Tb:YAG) garnet at $T = 85$ K in an external magnetic field $H = 0.5$ T parallel to the crystallographic axis [001]. Inset: circularly-polarized components of the light intensity σ_+ (solid line) and σ_- (dotted line) of the luminescence lines 1 and 2 of the $^5D_4 \rightarrow {}^7F_6$ emission band in a longitudinal magnetic field $H = 0.7$ T parallel to the crystallographic axis [001].

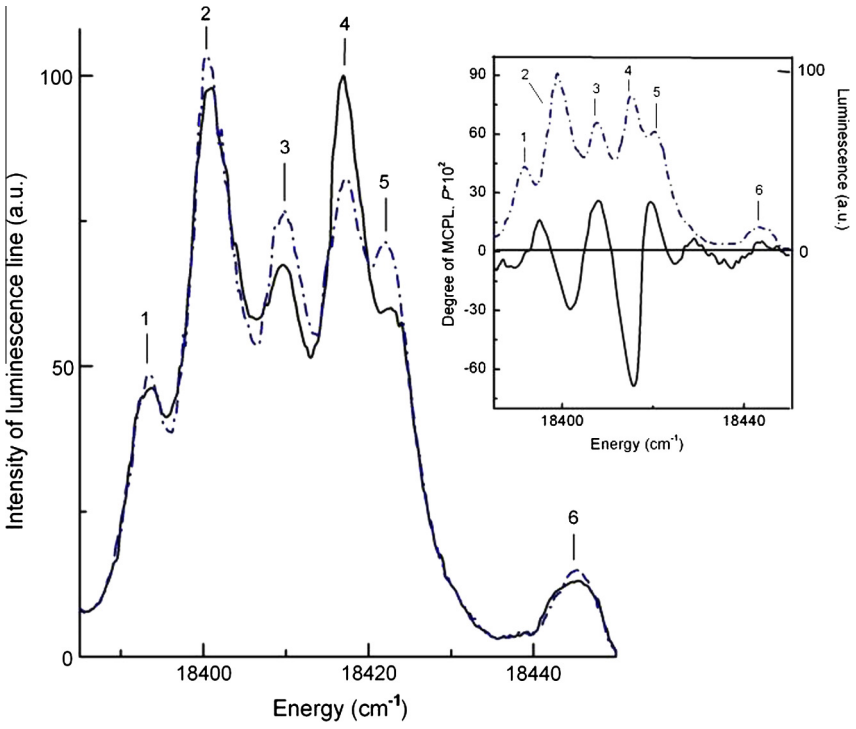

Fig. 3. Comparison of the MCPL degree P spectrum (solid line) with the luminescence (fluorescence) spectrum (dashed line) measured within the emissive $^5D_4 \rightarrow {}^7F_5$ band in the Tb^{3+}:$Y_3Ga_5O_{12}$ (Tb:YGG) garnet at $T = 85$ K in the external magnetic field $H = 0.5$ T parallel to the arbitrary crystallographic direction. Inset: circularly-polarized components of the light intensity (solid line) and σ_- (dotted line) of the luminescence lines 1, 2,..7 of the $^5D_4 \rightarrow {}^7F_5$ emission band in a longitudinal magnetic field $H = 0.7$ T parallel to the arbitrary crystallographic direction.

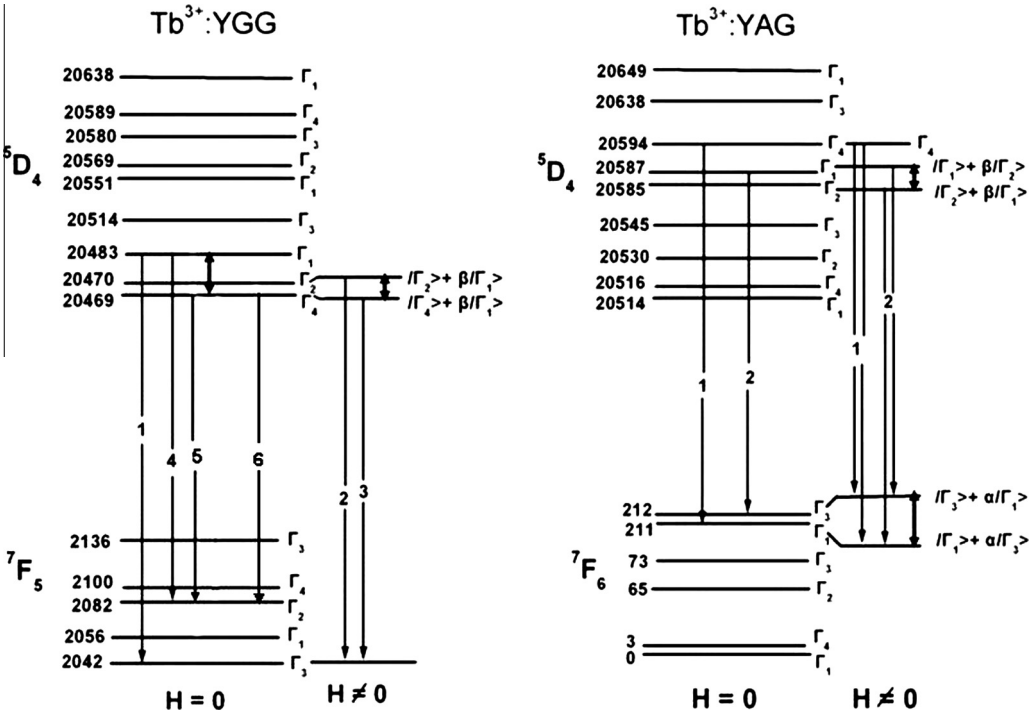

Fig. 4. Schematic diagrams of the optical transitions between Stark components of the $^7F_5$, $^7F_6$ and $^5D_4$ multiplet manifolds of the non-Kramers Tb^{3+} ion doped in YGG (on the left) and YAG (on the right). The $4f \rightarrow 4f$ emission transitions between the Stark sublevels are denoted by enumerated vertical arrows (transition numbers correspond to enumerated emission lines in Figs. 2 and 3). Stark level energies and their irreps Γi ($i = 1,2,3,4$) of the $^5D_4$ and $^7F_6$ multiplet manifolds of Tb^{3+} are given according to [23]; analogous values and symmetry labels of $^5D_4$ and $^7F_5$ multiplet manifolds sublevels for Tb^{3+} in the YGG structure were obtained from CF-calculations carried out in the present work. Magneto-optically-active radiative transitions between "mixed" states are shown on the right of each scheme of the optical transitions, with "mixing" of the quasidoublet states are shown by arrows.

study and directions and designations of axes of the local coordinate system, corresponding to one of crystallographically non-equivalent positions (*c*-sites) of the Tb^{3+} ion in garnet structure, are the same as in [5,8,11].

The observed luminescence of the Tb^{3+} ions is strongest specifically in the "blue" (from 20,370 to 20,430 cm^{-1}) and "green" (from 18,385 to 18,450 cm^{-1}) emission bands in Tb:YAG ($Tb_{0.2}Y_{2.8}Al_5O_{12}$) and Tb:YGG at $T = 85$ K, respectively. Detailed examination of the MCPL degree spectral dependences recorded for the emissive transitions $^5D_4 \rightarrow {}^7F_5$ in Tb:YGG and $^5D_4 \rightarrow {}^7F_5$ Tb:YAG and presented in Figs. 2 and 3 show differences between the energy level structure of these two systems (see Fig. 4), resulting in different MCPL signals.

As seen in Fig. 2, the spectral dependences of the MCPL degree P of the garnet $Tb_{0.2}Y_{2.8}Al_5O_{12}$ recorded on the lines 1 and 2 of the luminescence band $^5D_4 \rightarrow {}^7F_6$ at $T = 85$ K can be approximated by the sloping linear dependence within the corresponding luminescence lines, with the change of sign of the effect at the centers of the corresponding emission lines. The indicated spectral dependence features of the MCPL degree for lines 1 and 2 are characteristic of "diamagnetic" A'-terms of the MCPL degree for the non-Kramers ion [7,23]. This is confirmed by direct observation of the Zeeman splitting of the luminescence lines under consideration in the longitudinal external magnetic field $H = 0.7\ T$ at $T = 85$ K (see inset in Fig. 2).

By contrast, the MCPL spectral dependence for the emissive transition $^5D_4 \rightarrow {}^7F_5$ in Tb^{3+}:YGG (see Fig. 3) yields extrema of the MCPL signal coincident with the maximums of luminescence lines 2, 3 and 4, caused by different intensities of these lines in opposite circular polarizations in an external magnetic field (see Fig. 3 inset). A similar magneto-optical effect has been observed in the circularly polarized luminescence of erbium-yttrium aluminum garnet [24], where the corresponding extrema of the MCPL degree coincided with the centers of the Er^{3+} luminescence lines.

The differing MCPL phenomena in non-Kramers ions, such as Tb^{3+} and Ho^{3+}, in the garnet structure can be understood by taking into account wavefunction "mixing" by the external magnetic field of quasidoublet states from (or to) which the optical transitions take place. The low site symmetry does not allow us to use traditional mechanisms of MOA (i.e. "paramagnetic" *C*- and "diamagnetic" *A*-terms) to explain the observed MCPL experimental data. Therefore, we follow the work of Richardson et al. [25], which shows that the "mixing" of the wavefunctions of relatively closely spaced (10–20 cm^{-1}) Stark singlets in the energy spectrum of the ion by an external magnetic field H plays a significant role in the magneto-optics of the non-Kramers ions. This "mixing" results in magnetic moments for the "mixed" states and, as a consequence, the simultaneous appearance of the so-called "pseudo" C (or C') and "pseudo" A (or A') terms of the MOA in the non-Kramers ion [20].

According to the approach developed by Richardson et al. [25]:

(a) If the external magnetic field "mixes" the wavefunctions $<n|$ and $<\alpha|$ of two initial states i of the emissive transition energy levels, then the emissive transition probabilities for the left- and right-circularly polarized emission can be represented as:

$$W_{if}^{\pm} = \frac{\omega_0^3}{8\pi^2 c^3 \hbar^2 \bar{n}^2}\left[\sum_{o,n}(|<n|\hat{D}_X|o>|^2 + |<n|\hat{D}_Y|o>|^2) \mp \sum_{\alpha\neq n,o}\frac{2\mathrm{Im}[<\alpha|\hat{\mu}_Z|n> H}{\Delta_{\alpha n}}\Big(<o|\hat{D}_X|\alpha><n|\hat{D}_Y|o> - <o|\hat{D}_Y|\alpha><n|\hat{D}_X|o>\Big)\right] \quad (7)$$

where $\hat{\mu}_z$ is the z-component of magnetic moment, which arises only during the "mixing" by an external magnetic field H, is the energy interval between the "mixing" states of the Stark sublevels of the initial state of transition, $<o|$ is the wavefunction of the emissive transition final state, ω_0 is the average frequency of emissive transition, $\bar{n}$ is the average value of the index of refraction, and $\hat{D}_{X,Y}$ are the x- and y-components of the electric-dipole moment.

(b) Similarly, if the external magnetic field "mixes" the wavefunctions $|o>$ and $|\alpha>$ of two final states f of the emissive transition energy levels, we can write the expression for the emissive transition probabilities for the left- and right-circularly polarized emission as:

$$W_{if}^{\pm} = \frac{\omega_0^3}{8\pi^2 c^3 \hbar^2 \bar{n}^2}\left[\sum_{o,n}(|<n|\hat{D}_X|o>|^2 + |<n|\hat{D}_Y|o>|^2) \mp \sum_{\alpha\neq n,o}\frac{2\cdot \mathrm{Im}<\alpha|\hat{\mu}_Z|o> H}{\Delta_{o\alpha}}(<n|\hat{D}_X|\alpha><o|\hat{D}_Y|n> - <n|\hat{D}_Y|\alpha><o|\hat{D}_X|n>)\right] \quad (8)$$

where $\Delta_{o\alpha} = (E_o - E_\alpha)$ is the energy interval between the "mixing" states of the Stark sublevels of the final state of emissive transition.The circularly-polarized emission intensities $I_\pm$ are related to the corresponding transition rates $W_{if}^{\pm}$ by the following relation [25]:

$$I_\pm = \hbar\omega_0 \cdot N_{n'} \cdot W_{if}^{\pm} \cdot f(\omega, \omega_0') \quad (9)$$

where $N_{n'}$ is the number of ions in the emitting (initial) state proportional to its Boltsmann population and $f(\omega, \omega_0')$ is a normalized line shape function (Lorentz or Gauss) centered at ω_0. Note that the quantities and $f(\omega, \omega_0')$ are magnetic field H dependent. Using Eqns. (7) and (9), and taking into account the transformational properties of the symmetry group D_2 [5–7], we can find the expression for the resulting B-term of MCPL degree arising at the "mixing" of the wavefunctions $<n|$ and $<\alpha|$ of two initial closely located Stark levels, corresponding to the case of *a*), with accuracy to within the first order terms linear in and $\Delta_{\alpha n}/kT$:

$$P_B = \frac{\Delta I}{I} = \frac{I_- - I_+}{I_- + I_+} = \sum_{\alpha\neq n,o}\frac{2H\mathrm{Im}[<\alpha|\hat{\mu}_Z|n><o|\hat{D}_X|\alpha><n|\hat{D}_Y|o>](\rho_n - \rho_\alpha)}{\Delta_{\alpha n}(D_1\rho_n + D_2\rho_\alpha)} \quad (10)$$

$$D_1 = \frac{(|<n|\hat{D}_X|o>|^2 + |<n|\hat{D}_Y|o>|^2)}{2}, \text{ and}$$

$$D_2 = \frac{(|<\alpha|\hat{D}_X|o>|^2 + |<\alpha|\hat{D}_Y|o>|^2)}{2}$$

where P_B is the "mixing" B-term of the MCPL degree of the non-Kramers ion; is the zero-field Boltzmann population of the corresponding emitting state; D_1 and D_2 are the "dipole strengths" of emissive transitions from "mixed" by field H the states n and α to the final state o, respectively.Then for the important case, we can obtain the expression from (10) for the C'-term of MCPL degree corresponding to the emissive magneto-optical transition "quasidoublet → isolated singlet":

$$P_C = \frac{1}{kT}\frac{C'\cdot H}{(D_1 + D_2)} = \sum_{\alpha\neq n,o}\frac{2H\mathrm{Im}[<\alpha|\hat{\mu}_Z|n><o|\hat{D}_X|\alpha><n|\hat{D}_Y|o>]}{kT\cdot(D_1 + D_2)} \quad (11)$$

Using Eqs. (8) and (9) and assuming a Gaussian contour of the luminescence line, we can show that in case of (*b*) the expression for the-term of MCPL degree corresponding to the emissive magneto-optical transition "isolated singlet → quasidoublet" can be represented with accuracy to within the first order terms linear in $\mu_B H/\hbar\Gamma$ as:

$$P_A = \frac{(\omega_o - \omega)}{2} \cdot \frac{A' \cdot H}{(D_1 + D_2)} = \frac{(\omega_o - \omega)}{\Gamma^2} \cdot \sum_{\alpha \neq n,o} \frac{2H\mathrm{Im}[<\alpha|\hat{\mu}_Z|o><n|\hat{D}_X|\alpha><o|\hat{D}_Y|n>]}{(D_1 + D_2)} \quad (12)$$

where P_A is the "diamagnetic" A'-term of the MCPL of the non-Kramers ion; Γ is the luminescence line half-width (defined at $I = I_o/e$); and and D_2 are the "dipole strengths" of emissive transitions from initial state n to the final states α and o "mixed" by the external field H, respectively.

Thus, both the C'- and A'-terms of the MCPL degree are proportional to the product of the matrix elements of the transitions: electric-dipole from Stark sublevels of a quasidoublet (or singlet) of the initial state to a singlet (or quasidoublet) of the magneto-optical transition final state, and magnetic-dipole between "mixed" states of the same quasidoublets. If the magnetic-dipole (MD) transition between "mixing" states of the quasidoublets (α, n) or (α, o) is allowed, then the symmetry of the states in allowed transitions can be found by applying to the relations (10)–(12) the familiar selection rules in symmetry (considering the transformation properties of the point group of symmetry D_2) for matrix elements of the components of the dipole moment [5,6].

For example, according to the selection rules (in symmetry) applied to Eq. (12), the features of the MCPL degree spectrum of the garnet $Tb_{0.2}Y_{2.8}Al_5O_{12}$ associated with lines 1 and 2 of the luminescence band $^5D_4 \rightarrow {}^7F_6$ are caused by the emissive magneto-optically-active $4f \rightarrow 4f$ transitions: $^5D_4(\Gamma_4) \rightarrow {}^7F_6(\Gamma_1, \Gamma_3)$ and $^5D_4(\Gamma_1, \Gamma_2) \rightarrow {}^7F_6(\Gamma_1, \Gamma_3)$, respectively, between Stark sublevels of the $^5D_4$ and $^7F_6$ multiplet manifolds of the Tb^{3+} ion in D_2 symmetry. Taking into account that luminescence line 1 corresponds to the magneto-optically-active $4f \rightarrow 4f$ transition $^5D_4(\Gamma_4) \rightarrow {}^7F_6(\Gamma_1, \Gamma_3)$ of the "isolated singlet → quasidoublet" type, we can determine the Zeeman splitting value Δ_{Zeem} of the quasidoublet state (Γ_1, Γ_3) located at 212 cm^{-1} in the energy spectrum of ground $^7F_6$ multiplet (see Fig. 4). Using the experimental data given in Fig. 2 (see inset), we find that the Zeeman splitting of the $^7F_6$ (Γ_1, Γ_3) quasidoublet is $\Delta_{Zeem} = 2.4$ cm^{-1} in an external magnetic

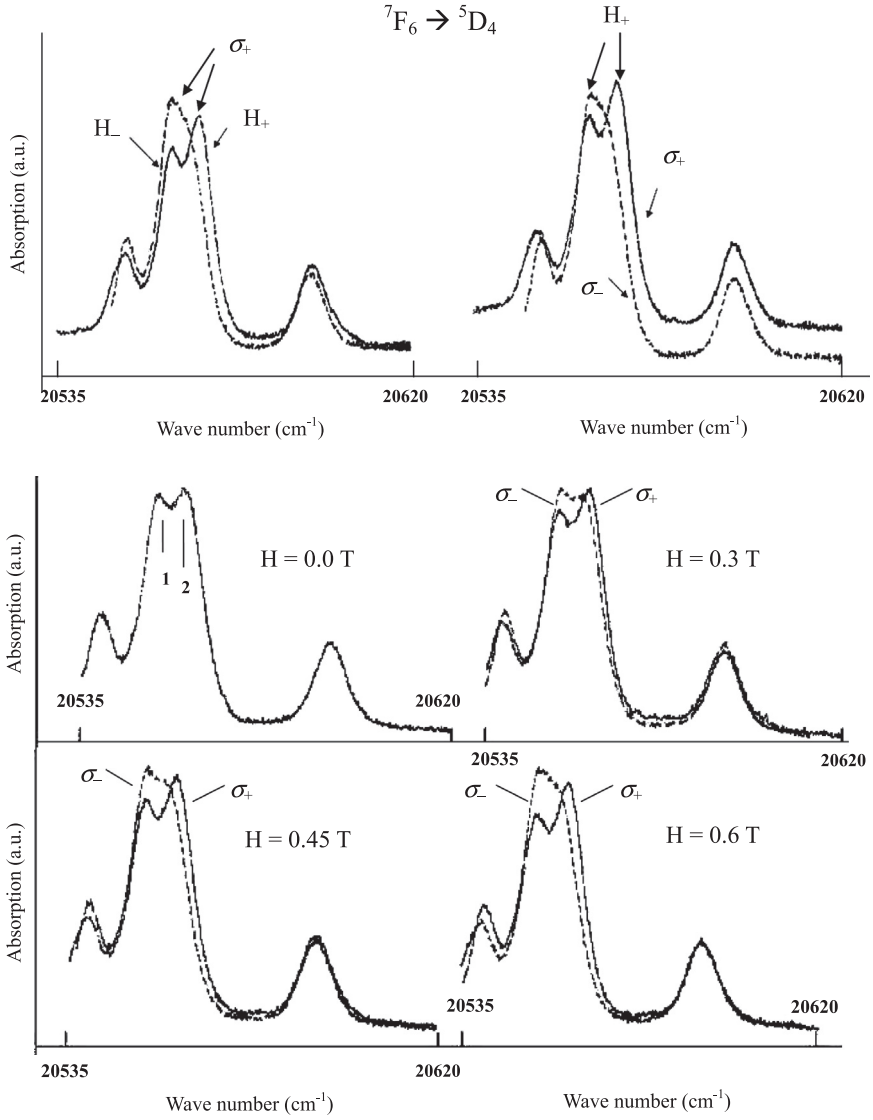

Fig. 5. The spectral dependence of the Zeeman splittings of the doublet absorption lines 1 (~20,563 cm^{-1}) and 2 (~20,570 cm^{-1}) at $T = 85$ K in an external magnetic field $H = 0.7$ T oriented along the crystallographic direction [1 1 0] of the TbGG crystal. The top two panels show the equivalence of splittings recorded at the circular polarization sign changing (for fixed external field direction) and at the external field sign changing (for the fixed circular polarization sign). Zeeman splitting field dependences of the doublet absorption lines recorded for left/right circular polarizations () at $T = 85$ K for a changing external magnetic field H (|| [1 1 0] axis) are shown at the bottom four panels of the figure.

field $H = 0.68\ T$. This corresponds to a g-tensor z-component for this quasidoublet of 15.2. This is consistent with the value $g_Z = 15.5$ found from numerical calculations of the Tb^{3+} energy spectrum of the $^7F_6$ multiplet [23].

For the emission transition $^5D_4 \rightarrow {}^7F_5$ (see Fig. 3), the spectral dependence of MCPL degree in Tb:YGG shows the "mixed" states of the lowest Stark quasi-doublet (Γ_2, Γ_4), and the next excited singlet (Γ_1) significantly affects the intensities $I_\pm$ of luminescence lines 2 and 3 only if the final state of the symmetry-allowed emissive transitions $^5D_4(\Gamma_1, \Gamma_4) \rightarrow {}^7F_5(\Gamma_3)$ and $^5D_4(\Gamma_1, \Gamma_2) \rightarrow {}^7F_5(\Gamma_3)$ is the ground Stark singlet Γ_3 of the $^7F_5$ multiplet at about 2042 cm^{-1} in Tb:YGG. This can be obtained by applying the symmetry selection rules to the MD- and ED-transition matrix elements in expression (10) for the B-term of MCPL degree. On the other hand, an appearance of the B-term of MCPL degree on the lines 4 and 5 (Fig. 3) is related with emissive magneto-optically-active $4f \rightarrow 4f$ transitions: $^5D_4(\Gamma_1, \Gamma_4) \rightarrow {}^7F_5(\Gamma_2)$ arising through "mixing" by the external magnetic field H of the closely spaced Stark sublevels Γ_4 and Γ_1 of the $^5D_4$ multiplet (see Fig. 4).

3.3. UV and visible Zeeman spectra of Tb^{3+} in TbGG

The spectral dependences of the longitudinal Zeeman effect of the TbGG paramagnetic garnet recorded for the absorption bands of the $4f \rightarrow 4f$ transitions $^7F_6 \rightarrow {}^5D_4$ and $^7F_6 \rightarrow {}^5L_{10}$ at $T = 85$ K are presented in Figs. 5 and 6, respectively. The Zeeman splitting field dependence for peaks 1 and 2 of the doublet line observed around 20,555 cm^{-1} show several interesting features. With an increasing longitudinal magnetic field H, we observe an increase in the energy separation between the doublet components 1 and 2 in the right circular polarization σ_+ of the light traveling parallel to the [1 1 0] axis of the crystal (see the bottom four panels of Fig. 5). At the same time, the energy separation between the doublet components decreases in the left circular polarization σ_- of the light, with the components overlapping almost for an external magnetic field of 0.6 T. This same behavior can be evoked in the spectra of a single circular polarization by reversing the magnetic field, as shown in the first panel of Fig. 5.

A similar effect is seen in the doublet line at about 26,760 cm^{-1} for the $^7F_6 \rightarrow {}^5L_{10}$ transition. Fig. 6 presents the left- and right-circular spectra taken at $T = 85$ K in a longitudinal magnetic field $H = 0.7\ T$ applied along the [1 1 0] crystallographic axis of TbGG crystal. From this figure, it can be seen that the doublet components 1 and 2 almost completely overlap in the left circular polarization spectrum, while the energy distance between same components increases in the right circular polarization σ_+ spectrum. Decomposition of the complex contour of this doublet line into Gaussian-type components [26] has shown that this phenomenon is essentially due to a decrease in the Zeeman splitting of the doublet components 1 and 2 in the left circular polarization σ_- with increasing magnetic field H, as shown in Fig. 5. It should be noted that experimental determination of the Zeeman splitting values for the doublet line at ~26,760 cm^{-1} is rather complicated, owing to the substantial initial overlap at $H = 0$ of the doublet components.

Given that we have previously obtained analogous results [18], we look for a simple explanation of an anomalous behavior of the Zeeman splitting in TbGG. An examination of the calculated Stark sublevel energies of the $^7F_6$ and $^5L_{10}$ multiplets (see Table 2) shows that the UV doublet line located near 26,760 cm^{-1} is caused by the $4f \rightarrow 4f$ transition between the ground state quasidoublet (Γ_1', Γ_3') of the $^7F_6$ multiplet and quasidoublet states (Γ_2', Γ_3') belonging to the excited $^5L_{10}$ multiplet. Therefore we can use the model of the magneto-optically-active $4f \rightarrow 4f$ transition "doublet – quasidoublet"

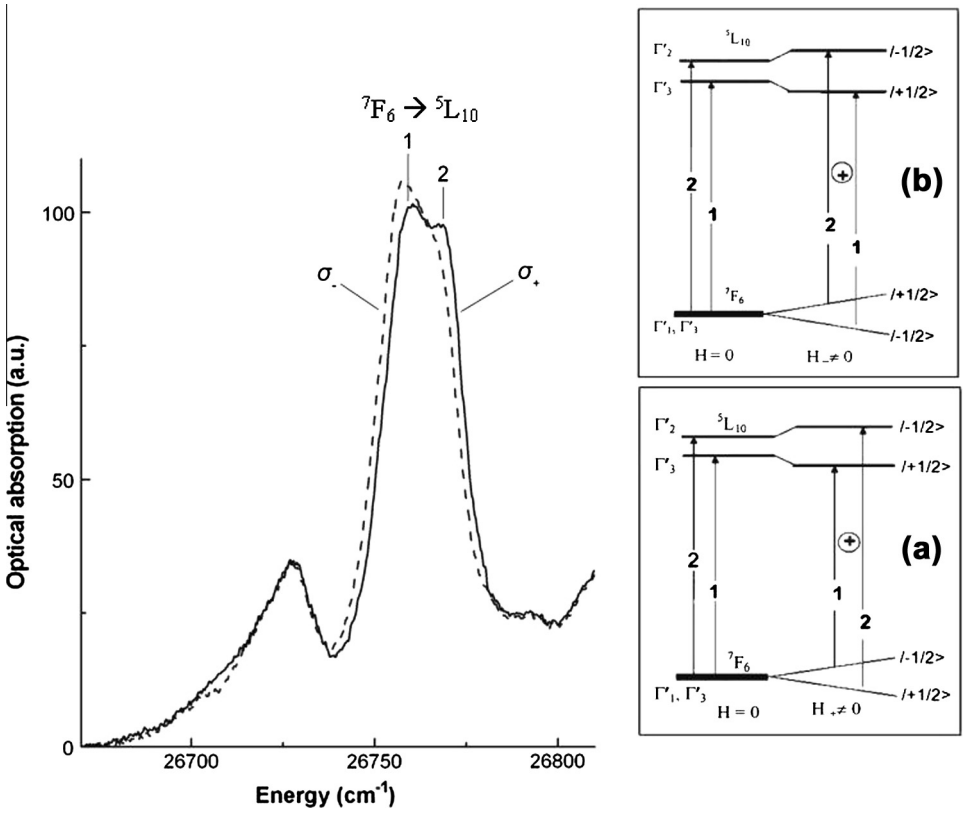

Fig. 6. Absorption of circularly polarized light in TbGG for doublet line observed at 26,760 cm^{-1} in which the light propagation and the magnetic field $H = 0.7\ T$ are parallel to the [1 1 0] crystallographic axis. The sample temperature is $T = 85$ K. Right circular polarization σ_+ is shown as a solid line; left circular polarization σ_- is shown as a dashed line. Inset: proposed explanation scheme of the longitudinal Zeeman effect for the doublet components 1 and 2 of this absorption line: (*a*) magnetic field H_+ applied along the direction of light propagation and (*b*) magnetic field applied in the opposite direction (H_-).

(previously proposed in [18]) with some simplified assumptions for the explanation above experimental data.

In the framework of this model, let's suppose that the ground state of the Tb^{3+} ion in YGG can be identified as a "conventional" doublet, since our modeling of the crystal-field split energy levels of non-Kramers Tb^{3+} ion in the gallium garnet predicts that the ground quasidoublet $^7F_6(\Gamma_1', \Gamma_3')$ has an initial splitting $\Delta_0 \approx 0.1\ cm^{-1}$ (see also Table 2), significantly smaller than the value of the Zeeman splitting (i.e., $\Delta_0 \ll g_{||}\mu_B H$, where $g_{||}$ is the quasi-doublet g-tensor component parallel to the external field H [6]). Therefore for the ground quasidoublet $^7F_6(\Gamma_1', \Gamma_3')$, the linear field dependence of the Zeeman splitting $\Delta(H)$ is similar to the behavior of the field dependence of the splitting for the conventional (pure) doublet of the "Ising" type (with), whose sublevels can be characterized by the wavefunctions |1/2, ±1/2>. As a consequence, under the action of the time-reversal operator $\hat{T}$ (which is equivalent to a change in the sign of the applied magnetic field $H \to -H$ for the non-Kramers ion [6]), the wavefunctions of the pure doublet (including Kramers doublets [6]) transform into each other, since $\hat{T}|+1/2> = +|-1/2>$ and $\hat{T}|-1/2> = -|+1/2>$ [6] (see inset in Fig. 6). The excited quasidoublet state $^5L_{10}$ (Γ_2', Γ_3') can be also identified as the state with "effective" angular momentum $J = 1/2$. But in this case, the wavefunctions and Ψ_2 of quasidoublet under the action of the time-reversal operator $\hat{T}$ remain unchanged, i.e. $\hat{T}|\Psi_1> = |\Psi_1>$ and $\hat{T}|\Psi_2> = |\Psi_2>$ [6] (see also inset in Fig. 6), due to the non-linear character of the Zeeman splitting field dependence, $\Delta(H)$, which can be written as: [6,18]. Note that the magnetic moment of the quasi-doublet is reoriented due to magnetization reversal, since this moment is induced by the external field H (Van Vleck paramagnetism [6,18]). At the same time, the magnetic moment of the conventional doublet is reoriented due to the inversion of the signs of the angular momentum projections of the doublet sublevels split by the applied magnetic field.

Using the difference in the mechanism of the magnetization reversal between the quasi-doublet and conventional doublet one can build the scheme of absorptive magneto-optically-active $4f \to 4f$ transitions occurring between Stark sublevels of the ground $^7F_6(\Gamma_1', \Gamma_3')$ and excited $^5L_{10}(\Gamma_2', \Gamma_3')$ states of the $4f^{(8)}$ configuration of Tb^{3+} (see inset in Fig. 6). Modeling schemes of magneto-optically-active transitions are given panels (a) and (b) of Fig. 6, where the equivalence of Zeeman splittings (Fig. 5) measured at the sign changing of the circular polarization (for fixed magnetic field direction) and at the sign changing of an external field (for fixed circular polarization sign) was used. An analysis of the Zeeman effect patterns shown in Fig. 6 (inset *a* and *b*) demonstrates that in an applied field H_+, the energy spacing between the absorption doublet line components 1 and 2 associated with the observed $4f \to 4f$ transitions in the right circular polarization σ_+ increases substantially. However, after the change of the magnetic field sign (i.e.,), at a fixed circular polarization σ_+ of light, the absorption lines begin to shift toward each other and the Zeeman splitting becomes zero at a field $H_- = 0.7\ T$.

Thus, consideration of the anomalous behavior of the Zeeman effect in TbGG shows that this effect can arise in the non-Kramers ion only for optical transitions between quasidoublet and "quasi-degenerate" states (with very small energy differences on the order of 0.1–0.2 cm^{-1}), which are equivalent to conventional (Kramers) doublets. These results show the significant difference between the remagnetization processes of non-Kramers quasidoublet states, on the one hand, and Kramers doublet states, on the other hand, that cannot be detected practically using traditional methods of magnetic measurements.

4. Conclusions

The results of this study of the optical and magneto-optical spectra of non-Kramers Tb^{3+} ion in the garnets $Tb_3Ga_5O_{12}$ (TbGG), $Y_3Ga_5O_{12}$ (YGG) and $Y_3Al_5O_{12}$ (YAG) allow us to make the following conclusions:

1. The intense optical absorption and the large MCD values observed in the Tb:YGG epitaxial thin film in the near UV spectrum at $T = 85$ K can be associated with spin and parity allowed electric-dipole transitions between the ground $^7F_6$ multiplet and the optically allowed ^7D state of the excited $4f^{(7)}5d$ configuration of Tb^{3+} in the garnet structure. Existence in the near UV region of allowed states of the excited $4f^{(7)}5d$ configuration of Tb^{3+} allow the possibility for effective energy transfer from these states to the high-energy states of Gd^{3+}, which is necessary for the successful realization of "quantum cascade emission" [27] (also called "quantum cutting" [28]).
2. Magneto-optical analysis confirms the reliability of the wavefunctions and their symmetry properties (i.e., irreps. of the D_2 symmetry group) obtained from crystal-field splitting calculations for the set of Stark sublevel eigenvectors belonging to $^7F_5$, $^7F_6$ and $^5D_4$ multiplet manifolds of Tb^{3+} in YAG and in YGG.
3. In the presence of an external magnetic field H, the "mixing" of the states of the lowest Stark singlets of the $^5D_4$ multiplet sublevels of the ground (Γ_2, Γ_4) quasi-doublet and of the closest excited singlet with the symmetry Γ_1, by an external magnetic field H in Tb:YGG significantly affects the intensities $I_\pm$ of luminescence lines 2 and 3 only if the final state of the symmetry-allowed radiative transitions $^5D_4(\Gamma_1, \Gamma_4) \to {}^7F_5(\Gamma_3)$ and $^5D_4(\Gamma_1, \Gamma_2) \to {}^7F_5(\Gamma_3)$ is the Stark singlet Γ_3 of the $^5D_4$ symmetry (the ground sublevel of the $^7F_5$ multiplet with an energy of about 2042 cm^{-1}).
4. The anomalous behavior of the Zeeman effect discovered in TbGG at $T = 85$ K in the UV absorption band $^7F_6 \to {}^5L_{10}$ clearly demonstrates the significant difference between the remagnetization processes of non-Kramers quasidoublet states and conventional Kramers doublet states, that cannot be detected practically using traditional methods of magnetic measurements.

Acknowledgements

This work was supported by the International Cooperation Program of the Ministry of Science and Technology of China under Grant 2011DFR50580.

References

[1] H.M. Crosswhite, H.W. Moos, Optical Properties of Ions in Crystals, Interscience, NewYork, 1967.
[2] A.A. Kaminskii, Crystalline Lasers: Physical Processes and Operating Schemes, CRC, New York, 1996.
[3] A.K. Zvezdin, A.V. Kotov, Modern Magneto-optics and Magnetooptical Materials, IOP Publishing, Bristol and Philadelphia, 1997. pp. 386.
[4] J.B. Gruber, B. Zandi, U.V. Valiev, Sh.A. Rakhimov, Phys. Rev. B 69 (2004) 115103.
[5] R. Baurer, J. Heber, D. Mateika, Z. Phys. B (Condensed Matter.) 64 (1986) 201.
[6] A.K. Zvezdin, V.M. Matveev, A.A. Mukhin, A.I. Popov, Rare-Earth Ions in Magnetically Ordered Crystals, "Mir", Moscow, 1985 (in Russian).
[7] U.V. Valiev, J.B. Gruber, G.W. Burdick, Magnetooptical Spectroscopy of the Rare-Earth Compounds: Development and Application, Scientific Research Publishing, USA, 2012. pp. 139.
[8] U.V. Valiev, U.R. Rustamov, B.Yu. Sokolov, V. Nekvasil, R.A. Rupp, M. Fally, I. Amin, Phys. Stat. Sol. (b). 231 (2002) 98.
[9] H.-J. Reyher, B. Faust, B. Sugg, R. Rupp, L. Ackermann, J. Phys. Condens Matter 9 (1997) 9065.
[10] G.W. Burdick, J.B. Gruber, K.L. Nash, S. Chandra, D.K. Sardar, Spectrosc. Lett. 43 (2010) 406.
[11] M. Guillot, A. Marchand, V. Nekvasil, F. Tcheou, J. Phys. C 18 (1985) 3547.
[12] H.A. Buckmaster, Can. J. Phys. 42 (1964) 386.
[13] Uygun V. Valiev, John B. Gruber, Fu Dejun, Vasiliy O. Pelenovich, Gary W. Burdick, Mariya E. Malysheva, J. Rare Earths 29 (2011) 776.
[14] J.B. Gruber, G.W. Burdick, U.V. Valiev, K.L. Nash, Sh.A. Rakhimov, D.K. Sardar, J. Appl. Phys. 106 (2009) 113110.

[15] V.S. Zapasskii, P.P. Feofilov, Sov. Phys. Usp. 18 (1975) 323.
[16] J. Badoz, M. Billardon, J.C. Canit, J. Russel, J. Opt. (Paris) 8 (1977) 373.
[17] U.V. Valiev, T. Asilov, R.A. Salyukov, Instrum. Exper. Tech. 37 (4(Part I)) (1994) 449.
[18] J.B. Gruber, D.K. Sardar, R.M. Yow, U.V. Valiev, A.K. Mukhammadiev, V Yu. Sokolov, I. Amin, K. Lengye, I.S. Kachur, V.G. Piryatinskaya, B. Zandi, J. Appl. Phys. 101 (2007) 023108.
[19] G.B. Scott, J.L. Page, J. Appl. Phys. 48 (1977) 1342.
[20] P.J. Stephens, Adv. Chem. Phys. 35 (1976) 197.
[21] C. Görller-Walrand, L. Fluyt, in: K.A. Gschneidner, Jr., L. Eyring (Eds.), Handbook on the Physics and Chemistry of Rare-Earths, vol. 40, Elsevier academic publishing company, North-Holland, Amsterdam, 2010, pp. 107 (Chapter 244).
[22] U.V. Valiev, G.S. Krinchik, S.B. Kruglyashov, R.Z. Levitin, K.M. Mukimov, V.N. Orlov, B.Yu. Sokolov, Fiz. Tverd. Tela 24 (1982) 2118.
[23] U.V. Valiev, J.B. Gruber, B. Zandi, U.R. Rustamov, A.S. Rakhmatov, D.R. Dzhuraev, N.M. Narzullaev, Phys. Stat. Sol. B 242 (2005) 933.
[24] Sh.A. Abdullaev, U.V. Valiev, B.Yu. Sokolov, Opt. Spectros. 87 (1999) 386. Translated from Opt. i Spektrosk. 87 (1999) 419.
[25] F.S. Richardson, J.P. Riehl, Chem. Rev. 77 (1977) 773.
[26] J. Badoz, M. Bollardon, A.C. Boccara, B. Briat, Symp. Farad. Soc. 3 (1969) 27.
[27] G.W. Burdick, M.F. Reid, in: K.A. Gschneidner, Jr., J.-C.G. Bunzli, V.K. Pecharsky (Eds.), Handbook on the Physics and Chemistry of Rare Earths, vol. 37, North-Holland, Amsterdam, 2007 (Chapter 232).
[28] K.D. Oskam, R.T. Wegh, H. Donker, E.V.D. van Loef, A. Meijerink, J. Alloys Comp. 300–301 (2000) 421.